PRESSURE AND CURRENT BALANCE CONDITIONS DURING ELECTRON BEAM INJECTIONS FROM SPACECRAFT

K. S. Hwang

Department of Mechanical Engineering
and Center for Space Plasma and Aeronomic Research
and
N. Singh
Department of Electrical and Computer Engineering
and Center for Space Plasma and Aeronomic Research
The University of Alabama in Huntsville
Huntsville, Alabama 35899

Abstract. Electrostatic charging level of a conducting surface in response to injections of electron beams into space plasma is investigated by means of one-dimensional Vlasov code. Injections of Maxwellian beams into a vacuum shows that the surface can charge up to an electric potential $\phi_s > W_b$, where W_b is the average electron beam energy. Since Maxwellian beams have extended tails with electrons having energies $> W_b$, it is difficult to quantify the charging level in terms of the energies of the injected electrons. In order to quantitatively understand the charging in excess of W_b, simulations were carried out for water-bag types of beam with velocity distribution functions described by $f(V) = A$ for $V_{min} \le V \le V_{max}$ and $f(V) = 0$ otherwise, where A is a constant making the normalized beam density unity. It is found that V_{max} does not directly determine the charging level. The pressure distribution in the electron sheath determines the electric field distribution near the surface. The electric field in turn determines the electrostatic potential of the vehicle. The pressure distribution is determined by the beam parameters such as the average beam velocity and the velocity spread of the beam.

Introduction

Electron beam injections from spacecrafts now constitute a major activity in space research. Already there are several experiments involving rockets ranging in altitude from about 100 kilometers to about 1500 km (e.g., see Review by Winckler (1980). During the STS-3 and Spacelab-2 missions of the shuttle, electron beam injections were carrieed out. These space experiments have revealed that in response to the injection a host of plasma processes are driven (Sasaki et al., 1986; Inan et al., 1984; and Shawhan et al., 1984). Low-altitude rocket experiments have shown that normally the rocket potential ϕ_s in response to the injection is considerably smaller than the injected electron beam energy W_b (Winckler, 1980). This is attributed to the effective neutralization of the charges on the vehicle by the return current from the ambient ionospheric plasma. At a low

ionospheric altitude, where neutral densities are significantly high ($\sim 10^8$ cm^{-3}), beam-plasma discharge provides an additional means for charge neutralization. On the other hand, high-altitude experiments have demonstrated that the vehicle can charge to potentials $\phi_s > W_b/e$, where e is the electronic charge (Managdze, 1983). The electron beam injections from the shuttle showed that when the current-collecting part of the shuttle was in the wake and an electron beam was injected, the vehicle charged to potentials $\phi_s \geq W_b/e$ (Sasaki et al., 1986).

Motivated by the experiments, there are now several numerical simulations on the electron beam injection. Parks et al. (1975) used a hydrodynamic approach to study the reflection of monoenergetic electron beam injected from a planar body into vacuum and showed that the reflection time $t_r \sim 2\omega_{pb}^{-1}$, where ω_{pb} is the electron-plasma frequency associated with the beam density n_b. Recently Pritchett and Winglee (1987), Okuda et al., (1987) and Okuda and Kan (1987) have used particle-in-cell code to investigate the dynamics of the injected beams. Winglee and Pritchett (1987) carried out simulations using particle codes emphasizing the temporal features of the injected electrons into an ambient plasma with density $n_a \ll n_b$. Singh and Hwang (1988) carried out simulations using Vlasov codes and dealt with the questions of the charging level of the vehicle when the ratio n_a/n_b is varied. They showed that when $n_a/n_b \gg 1$, the return current from the background plasma neutralizes the charge on the vehicle and the time-average vehicle potential and $\phi_{sa} \sim kT_e/e$ where k is the Bolzmann constant and T_e is electron temperature. On the other hand, when $n_b > n_a$, the plasma is not able to neutralize the charge and ϕ_{sa} can appreciably exceed the average beam energy. In this case, the electric potential distribution near the vehicle is like a thin sheath. In the intermediate case, when the vehicle potential lies in the range $kT_e/e \leq \phi_{sa} \leq W_b/e$, the beam penetrates into the plasma but much slower than the beam velocity. The propagation speed depends on the velocity of a triple-charge-layer structure which forms near the propagating beam head.

Despite several simulations, it is not clearly understood why vehicles charge to potentials $\phi_s > W_b/e$ (Managdze, 1983; and Machlem, 1988) when the ambient plasma is not able to effectively neutralize the positive charge on the vehicle. We have investigated this issue and we find that the electric field in the electron sheath near the vehicle is determined by the pressure balance. Since the pressure distribution does not only depend on the average beam velocity, but also on the beam temperature, density and self-consistent evolution of the plasma distribution in the electron sheath, it is difficult to predict analytically the dependence of the vehicle potential on the injected-beam parameters. Simulations of the injection of electron beams with water-bag types of velocity distribution functions with a sharp cut-off into a vacuum show that the charging level exceeds $(m/2e)V_{max}^2$, where V_{max} is the maximum velocity above which there are no electrons. This is in contrast

to the suggestion of Grard and Tunaley (1971), who assumed that for water-bag distributions of photoelectrons emitted from the surface, the surface potential $\phi_s = 1/2 \ (m/e) V_{max}^2$.

The rest of the paper is organized as follows. The numerical technique is described in section 2. In section 3, we have discussed the injection of Maxwellain and water-bag types of electron beams into both vacuum and ambient plasma. The paper is concluded in section 4.

Numerical Model

We model the electron beam injection by one-dimensional Vlasov simulations, in which the electron beam from a conducting surface at $X = 0$ is injected into a plasma of extent $0 < X \leq L$ as shown in Figure 1. The dynamics of the plasma particles and the self-consistent electric fields are determined by solving the coupled Vlasov and the Poisson equations. The positive charge at $X = 0$, resulting from the injection of the electron beam from this surface, is included in determining the electric fields. Any charge particles striking the surface is assumed to be lost, but their charges are added to the surface charges on the body. The surface electric field $E_x(x = 0)$ is determined by the net surface charge density. The plasma particles which exit the boundary at $X = L$ are reflected back into the system, simulating a uniform plasma. When the beam electrons begin to reach the surface at $X = L$, the simulation is stopped. At $X = L$, we use the Dirichlet boundary condition $\phi(X = L) = 0$, which is found to be good as long as the perturbations created by the electron beams do not reach this boundary.

In the simualations described here we use $L = 10^3 \lambda_d$, where λ_d is the Debye length with a reference plasma density n_0 and temperature T_e. We have used the electron to ion mass ratio for H^+. The numerical grids in X and V_x space are as follows: $\Delta X = \lambda_d$, ΔV_x for electrons is 0.25 V_t and for ions $0.05V_t$, where V_t is the electron thermal velocity with the temperature T_e. The time step to advance the solutions is $\Delta t = 0.1 \ \omega_{po}^{-1}$, where ω_{po} is the electron-plasma frequency with the density n_0. Further details about the simulation technique can be found in the work of Singh and Schunk (1984).

We have used the following normalizations: distance $\hat{X} = X/\lambda_d$, velocity $\hat{V} = V/V_t$, time $\hat{t} = t\omega_{po}$, current density $\hat{J} = J/J_t$, $J_t = en_0 V_t$, density $\hat{n} = n/n_0$, potential $\hat{\phi} = e\phi/T_e$, electric field $\hat{E} = E/E_0$, $E_0 = T_e/e\lambda_d$. In the case of electron beam injection into a vacuum, n_0 and T_e refer to the injected beam. When the beam injection occurs into an ambient plasma n_0 and T_e refer to the ambient plasma.

Numerical Results

We begin this section with the discussion on the injection of electron beams into a vacuum. Such an exercise throws a great deal of light on the causes for the vehicle charging considerably

in excess of W_b/e, where W_b is the average electron beam energy, $W_b = 1/2m_e V_b^2$. The results on the injection into an ambient plasma is described in the following section.

Injection Into Vacuum

Maxwellian Beams. The temporal evolution of the spacecraft potential for several velocities of Maxwellian beams are shown in Figure 2, in which $\hat{V}_b$ is the beam velocity normalized to its thermal velocity V_t. During the early stage ($t \leq 3\bar{\omega}_{pb}^{-1}$) the potential increases at a fast rate and then it settles down at a quasi-steady value depending on the average beam velocity. It is seen that the quasi-steady value of ϕ_s slowly increases. This is attributed to the fast electrons in the tail of the Maxwellian beam which continually escapes. The analytical calculation of Grard and Tunaley (1971) show an infinitely large potential when the ambient plasma is completely absent. The vehicle potential saturates at a time approximately given by

$$t_s \simeq 3\omega_{pb}^{-1} \tag{1}$$

This time is somewhat longer than the beam reversal time $t_r \simeq 2\omega_{pb}^{-1}$ calculated by Parks et al (1975), using a hydrodynamic treatment for the beam propagation. However, it should be noted that the t_r is the time when the beam velocity $V_b \to 0$ in the retarding potential distribution which t_s is the time when the reflected beam electrons reach the surface at $x = 0$ and effectively neutralize the further increase in the positive charge on it.

Figure 2 shows that the surface vehicle potential $\hat{\phi}_s$ increases with the average beam velocity $\hat{V}_b$. The dependence of $\hat{\phi}_s$ on $\hat{V}_b$ at $t = 3\bar{\omega}_{pb}^{-1}$ is plotted in Figure 3, which also shows the plot of $\hat{W}_b$ versus $\hat{V}_b$. Comparing the two curves in this figure we find that $\hat{\phi}_s \gg \hat{W}_b$. Intuitively it can be argued that in a Maxwellian beam with a finite temperature there are electrons at velocities $V > V_b$ and therefore $\hat{\phi}_s$ attains a value for which such fast electrons are also confined by the developing electric fields. But in a Maxwellian distribution there is no unique maximum velocity which can uniquely determine the maximum possible value of the surface potential $\hat{\phi}_s$.

Water-Bag Beams. In order to quantitatively understand the dependence of $\hat{\phi}_s$ on the energy of the injected electrons, we carried out simulations with water-bag type of distribution functions defined by

$$f_b(\hat{V}) = \begin{cases} A & \hat{V}_{min} \leq V \leq \hat{V}_{max} \\ 0 & \text{Otherwise} \end{cases} \tag{2}$$

where A is chosen so that the beam density is unity, namely,

$$A = \frac{1}{\hat{V}_{max} - \hat{V}_{min}} \tag{3}$$

The water-bag distribution functions have the attractive property that they have a sharp cut-off at $V = V_{max}$ with no electrons at $V > V_{max}$. Thus, simulations with such distributions can possibly show the dependence of ϕ_s on the maximum electron energy in the beam, which is not a well-defined quantity for a Maxwellian beam.

The solid curves in Figure 4 show the temporal evolution of the surface potential ϕ_s for two water-bag beams with the same average beam velocity $V_b = 6$, but V_{max} and V_{min} for the two beams are different. Beam #1 has $\hat{V}_{max} = 12$ and $\hat{V}_{min} = 0$, while for beam #2 $\hat{V}_{max} = 7$ and $\hat{V}_{min} = 5$. Beam #1 is warm while beam #2 is relatively cold. For beam #1, $\hat{\phi}_s = 170$ while for beam #2 $\hat{\phi}_s = 75$. These values far exceed the charging level determined by the maximum kinetic energies of the electrons in the two beams. These energies are

$$\hat{W}_{max} = \frac{1}{2} \hat{V}_{max}^2 = 72 , \quad \text{beam \#1} \tag{4}$$

$$\hat{W}_{max} = 24.5, \quad \text{beam \#2} \tag{5}$$

Grard and Tunaley (1971) have carried out analytical calculations on the charging of a plane surface in response to photoelectron emissions. They have considered a water-bag distribution for the emitted electrons. They have suggested that the charging level is determined by the maximum electron energy in the velocity distribution function. Our simulations show that this is not true as the surface charges to a potential greatly in excess of W_{max} (Figure 4). This authors used continuity and energy conservation equations

$$nV = n_0 V_0 \tag{6}$$

$$\frac{1}{2} mV^2 - e\phi = \frac{1}{2} mV_0^2 - e\phi_0 \tag{7}$$

and the Poisson equation to show that the surface electric field is given by

$$E_s^2 = \frac{2mN_s}{\epsilon_0} \int_0^\infty V^2 f_s(V) dV \qquad (8)$$

where $f_s(V)$ is the distribution function on the surface and N_s is the electron density there. In equations (6) and (7) n and V are the density and velocity where electric potential is ϕ and similarly n_0 and V_0 are the density and velocity where $\phi = \phi_0$.

We now compare these anlaytic results with our results obtained from the numerical simulations. In our normalized units equation (8) can be written as

$$\hat{E}_s^2 = 2\hat{N}_s \int_0^\infty \hat{V}^2 \, \bar{f}_s(\hat{V}) d\hat{V} \qquad (9)$$

where $\bar{f}_s(\hat{V})$ is one-sided distribution function and it is normalized to take into account both outgoing and incoming particles. We note that the integral in (9) is the effective electron temperature near the surface, if the average drift velocity is zero.

Figures 5a and 5b show the electron velocity distribution functions near the surface for beam #1 and #2 respectively. The effective electron temperature associated with the distribution functions is given by

$$\hat{T}_{eff} = \int_{-\infty}^\infty (\hat{V} - \hat{u})^2 \, f(\hat{V}) dV / \int_{-\infty}^\infty f(\hat{v}) d\hat{V} \qquad (10)$$

where $\hat{u}$ is the average drift velocity associated with the distributions. We find that near the surface for both the beams $\hat{T}_{eff}$ is about 25 (see Figure 7), and the electron density $\hat{N}_s = 2$ (see Figure 6). Substituting these values in (9), we obtain $\hat{E}_s = 10$, which is remarkably close to the electric fields obtained in the numerical simulations as shown in Figure 4 by the dotted curves. We find that despite this fair agreement on the surface electric fields obtained by theory and simulations, the surface potentials (ϕ_s) obtained from simulations greatly exceed those predicted by the theory (Grard and Tunaley, 1971). We now show that this difference is caused primarily by the pressure distribution in the electron sheath near the surface. We find that (7) is not valid throughout the electron sheath because it does not include the thermal energy.

The spatial distributions of density $\hat{N}(\hat{X})$, effective temperature $\hat{T}_{eff}(\hat{X})$ and electric field $\hat{E}(\hat{X})$ in the simulations for beam #1 and #2 are shown in Figures 6, 7 and 8, respectively. Using these distributions we now examine the relative contributions of the terms in the momentum balance equation,

325

$$\hat{u}\,\frac{\partial \hat{u}}{\partial \hat{x}} = -\hat{E} - \frac{1}{\hat{N}}\,\frac{\partial \hat{P}}{\partial \hat{X}} \tag{11}$$

where $\hat{u}$ is the average drift velocity and $\hat{P}$ is the pressure given by

$$\hat{P} = \hat{N}\,\hat{T}_e \tag{12}$$

If $\hat{u} = 0$, the electric field distribution is given by

$$\hat{E} = -\frac{1}{\hat{N}}\,\frac{\partial \hat{P}}{\partial \hat{X}} \tag{13}$$

In Figure 8, the solid and dashed curves show the numerically obtained spatial distributions of $\hat{E}$ for the two beams. The curve with the triangles is the electric field obtained from (13) for the beam #1. The pressure in (13) is obtained by the density and temperature shown in Figures 6 and 7, respectively. It is seen from Figure 8 that the electric field is quite accurately determined by the pressure force. This shows that the kinetic term $\hat{u}\,\partial \hat{u}/\partial \hat{x}$ is negligibly small in the momentum equation. This is expected from the nature of the distribution function in Figure 5a for beam #1.

The curve with circles (o-o) gives the plot of $\hat{N}^{-1}\,\partial \hat{P}/\partial \hat{X}$ for beam #2. It is seen that it slightly underestimates the electric field shown by the dashed curve. This is accounted by the fact that for the beam #2 the distribution function has distinct peaks (Figure 5b), which is not described well by an effective temperature.

The comparison of the electric fields directly obtained from the simulations with those derived from the pressure force clearly shows that it is the pressure force in the electron sheath which determines the electric field distribution and hence the surface potential of the vehicle. Comparing the electric field curves for the beam #1 and #2 in Figure 8, we see that the beam with the large V_{max} has relatively large electric fields extending to much greater distances than the beam with the smaller V_{max}. Thus, there is a dependence of charging on V_{max}, but it is not directly determined by the maximum electron energy $1/2\ m_e\ V_{max}^2$. The dependence is determined by the pressure distribution in the electron sheath. It is difficult to predict the pressure distribution because of the highly non-linear nature of the problem.

Effects of Ambient Plasma on Charging

The ambient plasma reduces the charging level by providing a return electron current, which partly neutralizes the positive charge on the surface. Figures 9a and 9b show the temporal

evolution of the surface potential for a Maxwellian beam with beam velocity $V_b = 6$ injected into ambient plasmas with densities $n_a = 0.1\ n_b$ and $0.2\ n_b$. The beam and ambient plasma temperatures are assumed to be the same. The effect of the ambient plasma on the surface potential is found to be twofold; it causes oscillations in the surface potential and the time average value of ϕ_s decreases with increasing ambient plasma density. Without any ambient plasma, the surface potential attained a quasi-steady value of about $\phi_s = 70$ (see Figure 3). For $n_a/n_b = 0.1$ and 0.2, its time-average values reduce to 50 and 45, respectively. However, it is important to note that for such small ambient plasma densities, the charging level exceeds considerably the average beam energy $W_b = 18$, and the beam does not propagate into the plasma.

The oscillations seen in Figure 9 in the surface potential are found to have time periods determined by the ambient plasma frequency. For example, the time periods seen in Figures 9a and 9b are $\tau = 20\ \omega_{pb}^{-1}$ and $14\omega_{pb}$, respectively, and they are given $\frac{2\pi}{\sqrt{(n_b/n_a)}}\ \omega_{pb}^{-1}$.

We have found that for sufficiently small beam densities when $\phi_{sa} \lesssim W_b$, the beam begins to penetrate into the plasma (Singh and Hwang, 1988). However, the propagation speed critically depends on the time-average surface potential ϕ_{sa}. When $\phi_s \sim (kT/e) \ll W_b$ for $n_a \gg n_b$, the beam propagates into the plasma with the injection velocity Singh and Hwang (1988). As ϕ_s increases with decreasing value of the relative ambient plasma density (n_a/n_b), the propagation velocity decreases. For surface potentials in the range $(kT/e) \ll \phi_s \lesssim W_b$, Singh and Hwang (1988) found that the beam head penetrates into the plasma with well-defined laminar potential structure near the beam head. The velocity of the potential structure is determined by the nonlinear plasma processes through which it evolves.

Conclusion

We have investigated in this paper the charging level of a conducting surface when an electron beam is injected from it. Injections into both vacuum and ambient plasma are considered. When a Maxwellian beam is injected into vacuum it is found that the surface charges to a potential much greater than the average beam energy. The dependence of the charging in excess of the average beam energy is investigated by considering beams with water-bag types of velocity distribution functions with distinct maximum velocity V_{max} such that no electron velocities $V > V_{max}$. It is found that the electric field distribution in the electron sheath near the surface is determined by the pressure distribution. Thus, the surface potential is determined not only by the V_{max}, but by all the beam parameters such as the density n_b, average beam velocity and the velocity spread of the beam. The parameters determine the pressure distribution in the electron sheath. Since the effective temperature and the density

distributions in the sheath evolve self-consistently through the nonlinear dynamics of the electrons, it is difficult to predict the charging level.

In our one-dimensional model, we have not included return currents coming from directions other than that for the beam injection. For the omnidirectional return current, the surface potential will in general tend to be smaller than that for the one-dimensional case. However, space experiments have shown that vehicles do charge to potentials comparable to, or in excess of, the average electron beam energy (Sasaki, et al. 1986, Managdz, 1983, Machlem, 1988). Therefore, the physical processes seen in the one-dimensional simulations are relevant to space experiments.

References

Grard, R. J. L. and J. K. E. Tunaley, Photoelectron sheath near a planar probe in interplanetary space, J. Geophysical Res., 75, 2498, 1971.

Inan, U. S., M. Pon, P. M. Banks, P. R. Williamson, W. J. Raitt and S. D. Shawhan, Modulated beam injection from the space shuttle during magnetic conjunctions of STS-3 with the DE-1 satellite, Radio Sci., 19, 487, 1984.

Managadze, G. G., Plasma processes in the region of electron beam injection from a high altitude payload, Active Experiments in Space Symposium at Alpach, 24-28 May 1983, Eur. Space Agency Spec. Publ., ESA SP-195, 161, 1983.

Okuda, H., and J. R. Kan, Injection of an electron beam into a plasma and spacecraft charging, Phys. Fluids, 30, 209, 1987.

Okuda, H. R. Horton, M. Ono, and M. Ashour-Abdalla, Propagation of a nonrelativistic electon beam in a plasma in a magnetic field, Phys. Fluids, 30, 200, 1987.

Parks, D. E., A. R. Wilson, and I. Katz, Monode plasma sheath dynamics T-NS 75, Dec., IEEE Trans. Nucl. Sci., 2368, 1975.

Prichett, P. L, and R. M. Winglee, Plasma environment during particle beam injection into space plasmas, 1, Electron beams, J. Geophys. Res., 92, 7673, 1987.

Sasaki, S. N. Kawashima, K. Kuriki, M. Yanagisawa, and T. Obayashi, Vehicle charging observed in SEPAC Space Lab-1 experiment, J. Spacecr. Rockets, 23 129, 1986.

Shawhan, S. D., G. B. Murphy, P. M. Banks, P. R. Williamson and W. J. Raitt, Wave emissions from dc and modulated electron beams on STS-3, Radio Sci., 19, 471, 1984.

Singh, N. and R. W. Schunk, Plasma response to the injection of an electron beam, Plasma Phys. Controlled Fusion, 26, 859, 1984.

Winckler, J.d R., The application of artificial electron beams to magnetospheric research, Rev. Geophys., 18, 659, 1980.

Winglee, R. M., and P. L. Prichett, Charging effects during the injection of dense electron beams, J. Geophys. Res., 92, 6114, 1987.
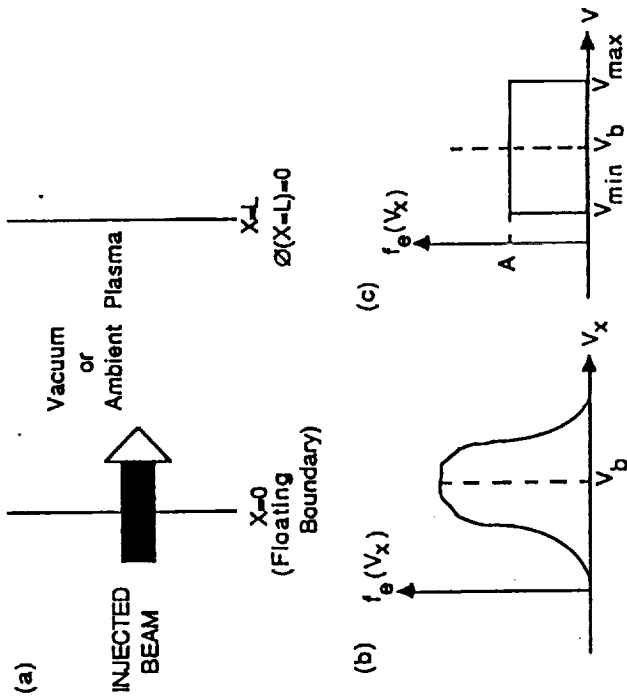
Spacecraft Potential vs. Time

Figure 2. Temporal evolution of the surface potential $\tilde{\phi}_s$ for Maxwellian beams with different beam velocities ($\tilde{V}_b$), which are normalized to the beam thermal velocity.

Figure 1. (a) simulation scheme; the electron beam is injected at the boundary x = 0. The region 0 ≤ x ≤ L is either vacuum or it contains an ambient plasma with density n_a and temperature T_a. The injected beams may have velocity distribution functions as shown in (b) Maxwellian distribution or in (c) water-bag distribution. The average beam velocity is V_b. At the right hand boundary the electric potential $\phi(x=d) = 0$ while the left hand boundary (x = 0) is kept floating.

329

Figure 3. Surface potential $\hat{\phi}_s$ as a function of beam velocity $\hat{V}_b$ for the beams injected into vacuum. Normalized beam energy $(1/2 \; \hat{V}^2{}_b)$ as a function of V_b is also shown.
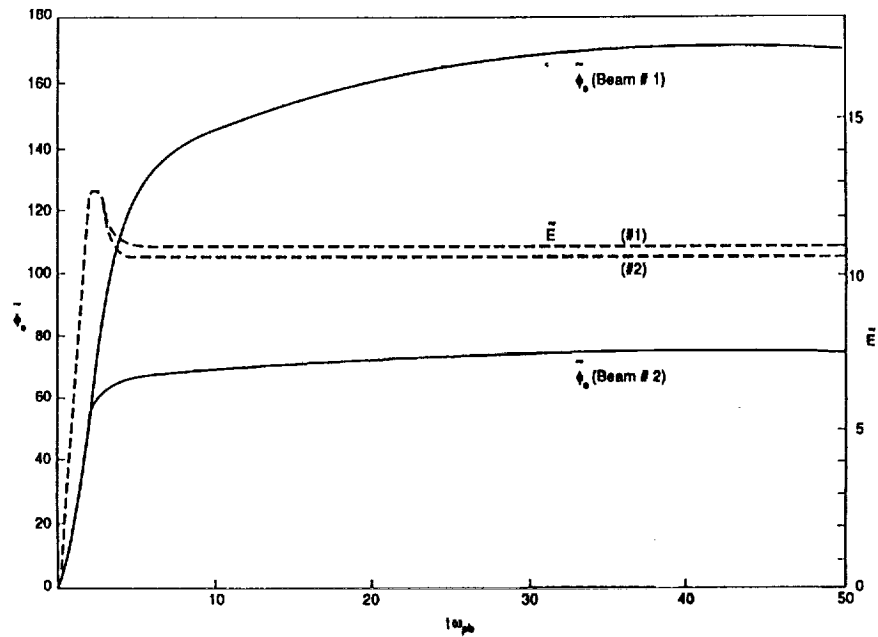

Figure 4. Temporal evolutions of surface potential ϕ_s and electric field $\hat{E}_s$ are shown for water-bag beams #1 and #2. For both the beams $\hat{V}_b = 6$; for beam #1 $\hat{V}_{min} = 0$, $\hat{V}_{max} = 12$ and for beam #2, $\hat{V}_{min} = 5$, $\hat{V}_{max} = 7$.
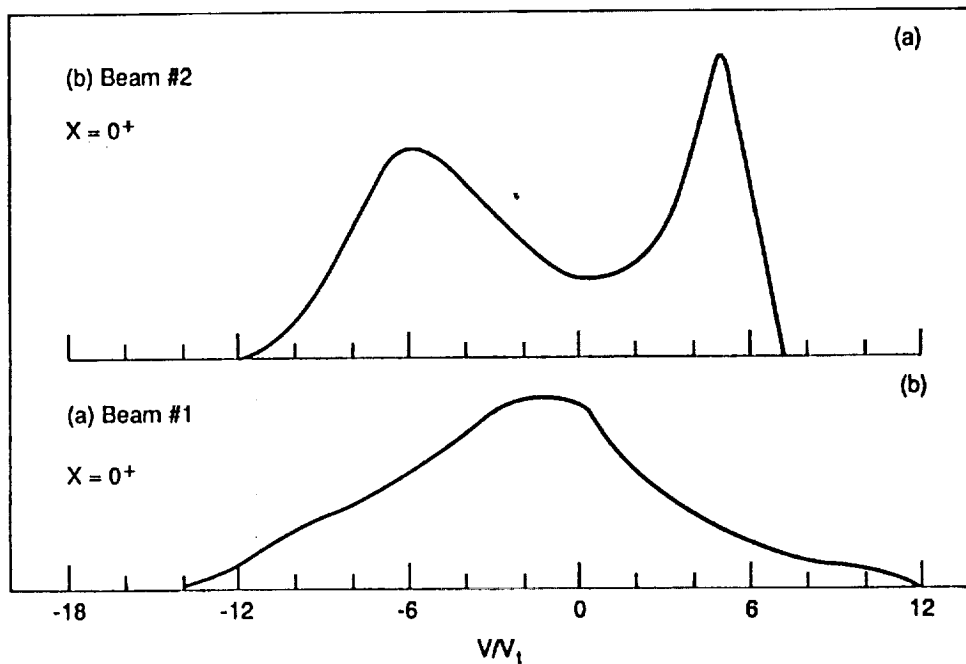
(b) Beam #2

X = 0⁺

(a) Beam #1

X = 0⁺

V/V_t

Figure 5. Electron velocity distribution functions near the surface $X = 0^+$ at $t\omega_{pb} = 50$. (a) beam #1, (b) beam #2. It is worth mentioning that the distribution functions shown are not exactly at $x = 0$, but they are at $x = 0^+$ as they are averaged over 2 grid spaces in front of the surface at $x = 0$. The distributions show that the injected water-bag beams have been modified by the intense electric fields near the surface.
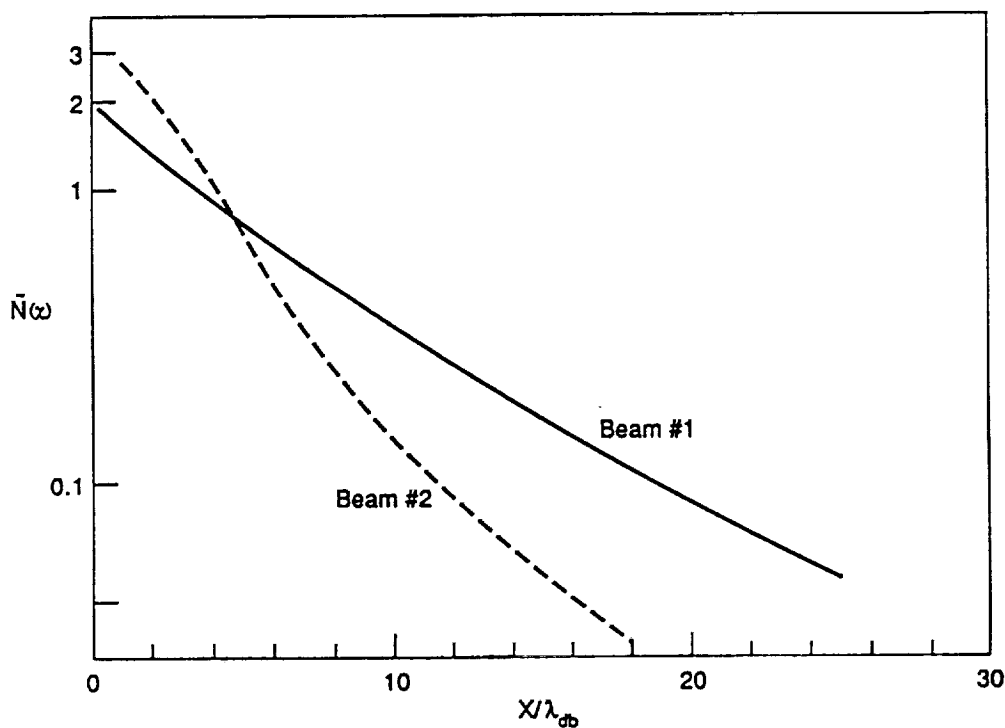

$\bar{N}(x)$

Beam #1

Beam #2

X/λ_{db}

Figure 6. Density distribution in the electron sheath for the water-bag beams #1 and #2.
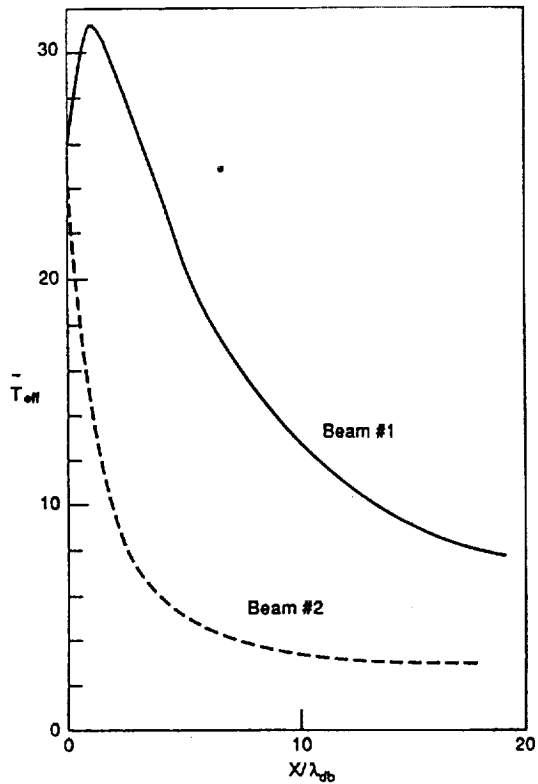
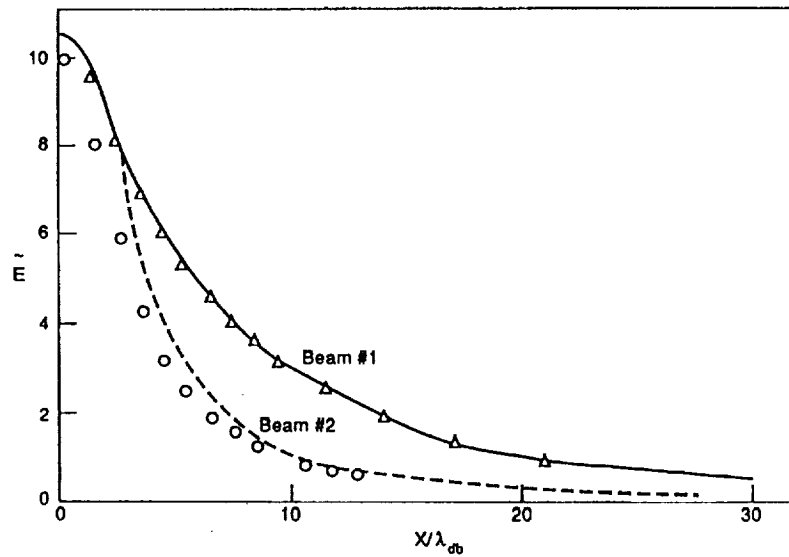Figure 7. Effective temperature distributions for the beam #1 and #2 in the electron sheath.

Figure 8. Electric field distributions. Beam #1: solid curve gives $\tilde{E}$ from numerical simulations and the triangles give the $\tilde{E}$ field from pressure balance. Beam #2: broken curve gives $\tilde{E}$ from simulation while the circles give $\tilde{E}$ field from pressure balance.
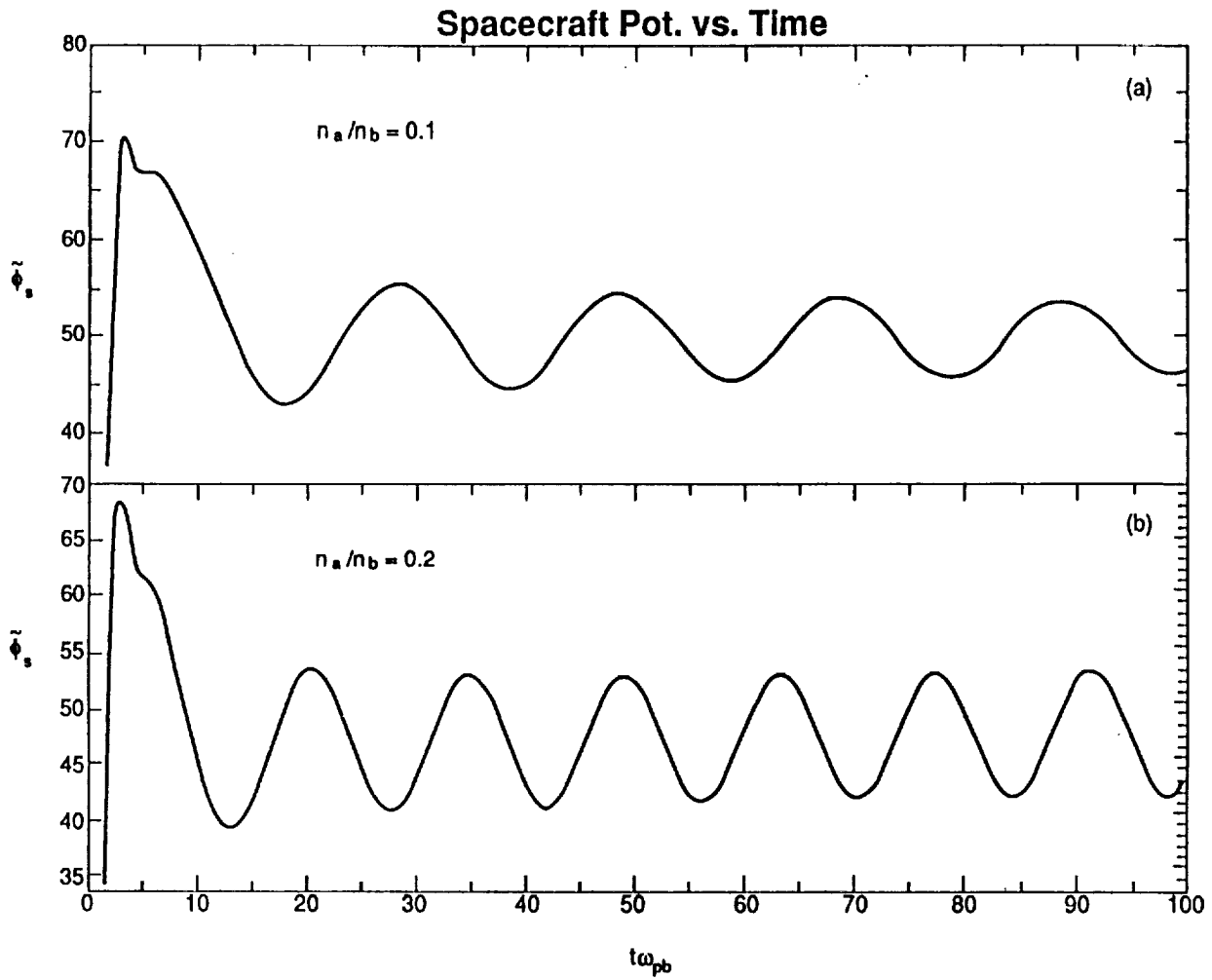
Figure 9. Temporal evolution of surface potential ϕ_s when Maxwellian beams are injected into ambient plasmas: (a) ambient plasma density $n_a = 0.1\, n_b$, (b) $n_a = 0.2\, n_b$; beam velocity $V_b = 6$.